

Research Article

NaY Zeolite Synthesis from Vermiculite and Modification with SurfactantThiago Rodrigo Barbosa Barros [†], Thianne Silva Batista Barbosa [†], Meiry Gláucia Freire Rodrigues ^{†, *}Universidade Federal de Campina Grande, Unidade Acadêmica de Engenharia Química, 58109-970 Campina Grande - PB, Brazil; E-Mails: thiagoidbarbosa@gmail.com; thianne.silva@gmail.com; meiry.freire@eq.ufcg.edu.br[†] These authors contributed equally to this work.^{*} **Correspondence:** Meiry Gláucia Freire Rodrigues; E-Mail: meiry.freire@eq.ufcg.edu.br**Academic Editor:** Angela Martins**Special Issue:** [Zeolite Materials and Catalysis](#)*Catalysis Research*

2023, volume 3, issue 4

doi:10.21926/cr.2304031

Received: October 24, 2023**Accepted:** December 18, 2023**Published:** December 26, 2023**Abstract**

This work focuses on preparing NaY zeolite using alternative sources of silica and modifying the zeolite with the surfactant cetyltrimethylammonium bromide. Two different hydrothermal synthesis routes were employed: the conventional method using sodium silicate as the silica source, and the other is a sustainable approach using vermiculite clay as the silica source. In traditional zeolite synthesis, sodium silicate is often used as the source of silica. However, . The vermiculite was subjected to an acid treatment, followed by a primary treatment to obtain silica. Using the ion exchange method, the NaY zeolite was modified by an organic surfactant CTABr. Based on the various characterization techniques, it was possible to verify the obtaining of NaY zeolite through the conventional and sustainable routes, in which the structural properties were maintained. They used the sustainable path to synthesize NaY zeolite, which allowed for obtaining a material with low synthesis cost and properties similar to those synthesized conventionally. The structures of the NaY zeolites were maintained after the modification process with the surfactant Cetyltrimethylammonium Bromide (CTABr), demonstrating the structural stability of the zeolites and the efficiency of the modification process.



© 2023 by the author. This is an open access article distributed under the conditions of the [Creative Commons by Attribution License](#), which permits unrestricted use, distribution, and reproduction in any medium or format, provided the original work is correctly cited.

Keywords

Vermiculite; NaY zeolite synthesis; hydrothermal method; cetyltrimethyl ammonium bromide (CTABr); ion exchange reaction; sustainable route

1. Introduction

The foundation of sustainability rests upon a fundamental and well-established truth: Every necessity for human survival and welfare is intricately linked, either directly or indirectly, to the natural environment [1]. The natural environment supplies the air we inhale, the water we consume, and the food we partake in. It fundamentally shapes our communities and the wellspring of renewable and nonrenewable resources essential to civilization. The quality of our environment is integral to our health, well-being, economy, and security [2].

Several research studies are underway to develop new materials for the adsorption of chemical pollutants from industries in general. Due to their physicochemical and morphological properties, zeolites stand out as promising materials that can be used in developing highly effective technologies to contribute to the preservation and sustainability of the environment [3-5].

Zeolites are aluminosilicates with a well-defined network structure, which includes cavities occupied by ions and water molecules, allowing considerable freedom of movement. The zeolite framework incorporates cations derived from either group I or II elements in the periodic table (e.g., Na⁺, K⁺, Mg²⁺, Ca²⁺), stabilizing the negative charges at exchangeable sites [Breck]. The mobile cations within the structure can exchange with other cations in the solution, while the intracrystalline zeolitic water can be reversibly removed [6].

For instance, cationic surfactants such as quaternary ammonium compounds (QACs), including cetyl trimethyl ammonium bromide (CTABr) with positively charged surfactant heads, can undergo adsorption onto zeolite via ion exchange with the surface and framework cations of the zeolite. Concerning the interaction of surfactant molecules with the zeolite, their size prevents them from entering the narrow pores, leading to their adherence to the external surfaces of the zeolite. Specifically, CTAB molecules, characterized by a head diameter of 0.694 nm [7], are unable to penetrate the average pore diameter of NaY zeolite (0.74 nm) [8]. As a result, these molecules would occupy the exchangeable active sites located on the exterior of the NaY zeolite framework [9].

Processes have been developed using clay minerals in search of more economical raw materials. These natural minerals provide natural sources of Al₂O₃ and SiO₂, replacing conventional chemical reagents such as sodium silicate and silica [10].

Clays are natural materials with low elasticity and density, finding diverse applications, such as the removal of heavy metals, the controlled release of drugs, petroleum bleaching, and the synthesis of molecular materials [11]. Vermiculite is a clay that belongs to the 2:1 layered phyllosilicate family and is one of the most promising and abundant in nature, often resulting from the exchange of mica through ion exchange in tri-octahedral smectites [12].

Clay minerals predominantly comprise aluminosilicates, suggesting they may be suitable raw materials for zeolite synthesis [13].

The synthesis of zeolites from laboratory chemicals is expensive. A currently available option to produce efficient and low-cost zeolites is using mineral materials rich in Si and Al, for example, clays [13].

Its high costs and environmental pollution constrain the widespread industrial production of the organic template method. The research focus has shifted to the organic template-free method for preparing high-silica Y zeolites [14].

Our research group has published studies on preparing molecular sieves with alternative silica sources [15-22].

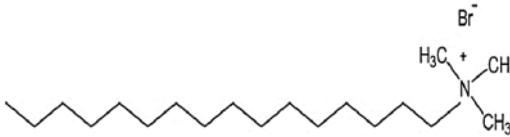
No prior literature has explored the utilization of vermiculite clay in synthesizing zeolites, rendering this study innovative. This study aims to utilize a sustainable silica source, namely vermiculite, for the synthesis of zeolite NaY. Two distinct approaches were employed: the conventional method utilizing sodium silicate as the silica source and the sustainable way using vermiculite clay as the silica source. The NaY- CTABr were prepared using the ion exchange method and were characterized by X-ray diffraction and FTIR. These materials (NaY- CTABr) can be a promising candidates in pharmaceutical and biomedical applications.

2. Materials and Methods

All chemicals and solvents were purchased from commercial suppliers and used as received, including Sodium Aluminate (NaAlO_2 , Sigma-Aldrich), Sodium Silicate (Na_2SiO_3 , Dinâmica), Sodium Hydroxide (NaOH , Cinética), Cetyltrimethylammonium Bromide ($\text{C}_{19}\text{H}_{42}\text{BrN}$, Dinâmica).

The properties of Cetyltrimethylammonium Bromide are given in Table 1.

Table 1 Properties of the Cetyltrimethylammonium Bromide.

	Molecular formula	Chemical structure	Molecular mass g/mol
Cetyltrimethylammonium Bromide	$\text{C}_{19}\text{H}_{42}\text{BrN}$		364.4

2.1 Vermiculite Clay Processing

Vermiculite clay, União Brasileira de Mineração, Santa Luzia-PB, Brazil) was sieved with a N° 200 (0.074 mm) sieve, according to a Brazilian ABNT standard.

To use vermiculite clay as a source of silica, previous and subsequent treatments were carried out to obtain the clay in a more reactive form. The first treatment was crushing its grains. After these physical processes, acid and essential therapies were carried out.

2.2 Acid Treatment of Vermiculite Clay (Leaching)

This procedure was carried out: a 3 mol/L hydrochloric acid solution was prepared, and vermiculite clay was added with a ratio of 1:10 clay mass to solution volume, under magnetic stirring, at 100°C for 2 h. Then, the material was separated by decantation. The final solid was washed with 2 L of deionized water, filtered until pH 7, and then dried in an oven at 100°C for 24 h [23].

The steps to be followed in the acid treatment are shown in the Scheme (Figure 1).

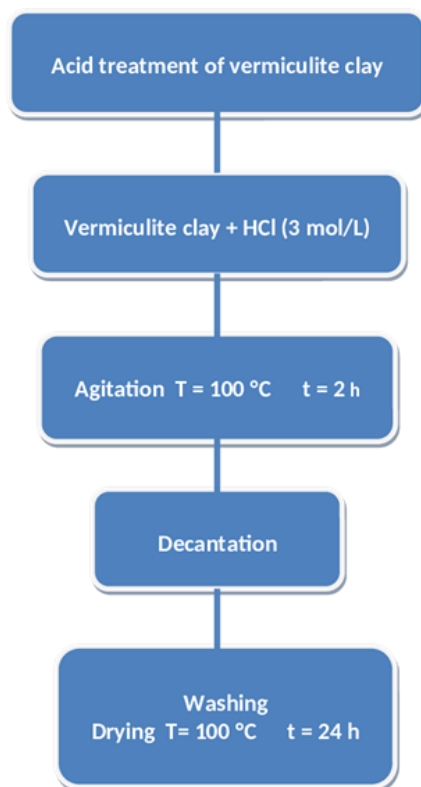


Figure 1 Scheme vermiculite clay acid treatment.

2.3 Basic Vermiculite Clay Treatment

After the acid treatment, the resulting material was subjected to a primary treatment. This procedure was carried out as follows: a 1 mol/L sodium hydroxide solution was prepared, and vermiculite clay was added with a ratio of 1:7 clay mass to volume of solution. The material was kept under stirring at 100°C for 6 h. Then, the answer was filtered, and the liquid part, the filtrate, was used for precipitation tests with 37% HCl. HCl was added to the filtrate until all the silica precipitated or until the solution reached pH 7. The precipitated silica was then dried at 100°C for 24 h and subsequently weighed, and from its mass, it was possible to determine the percentage of clay that could be dissolved in 6 h of primary treatment [24].

The steps to be followed in the primary treatment are shown in the Scheme (Figure 2).

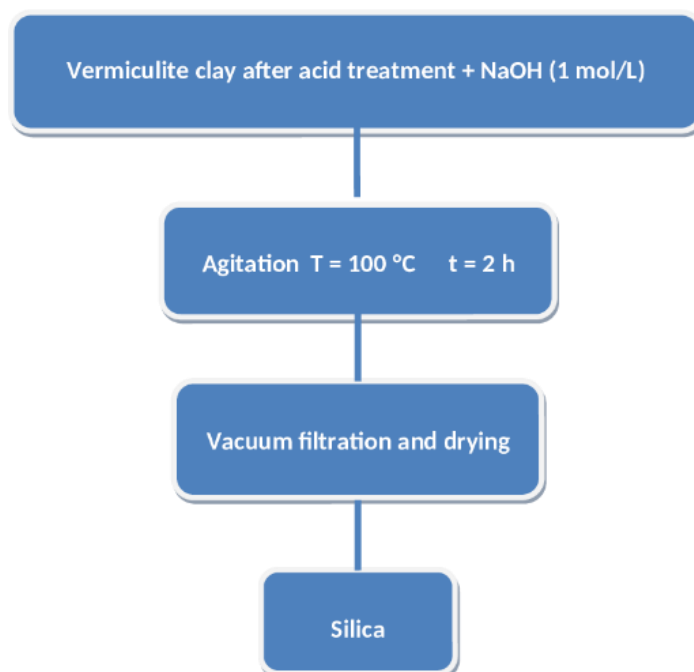


Figure 2 Scheme vermiculite clay basic treatment.

2.4 Synthesis of NaY Zeolite Via Conventional Route

The synthesis of NaY zeolite was carried out based on the methodology developed by the authors [25].

Two solutions were prepared to synthesize zeolite NaY: Solution 1 (sodium hydroxide, sodium aluminate, sodium silicate, and deionized water) and Solution 2 (sodium hydroxide, sodium aluminate, and deionized water). Solution 1 experienced a 24-hour aging process. After, the solution 1 was added slowly under agitation to the solution 2. The reaction mixture resulted in a milky solution of chemical composition: $4.6Na_2O:Al_2O_3:10SiO_2:180H_2O$. Then was placed in a stainless steel autoclave where the hydrothermal synthesis occurred at $90^\circ C$ for 7 h. After immersing the autoclaves in cold water, the resulting material was washed until $pH \leq 9$, and subsequently dried at $60^\circ C$ for 24 h.

The molar composition of the reaction mixture was $4.6Na_2O: Al_2O_3: 10SiO_2: 180H_2O$.

The sample was named NaY_C zeolite, taking into account the conventional method used.

The steps to be followed in synthesizing conventional NaY zeolite are shown in the diagram in Figure 3.

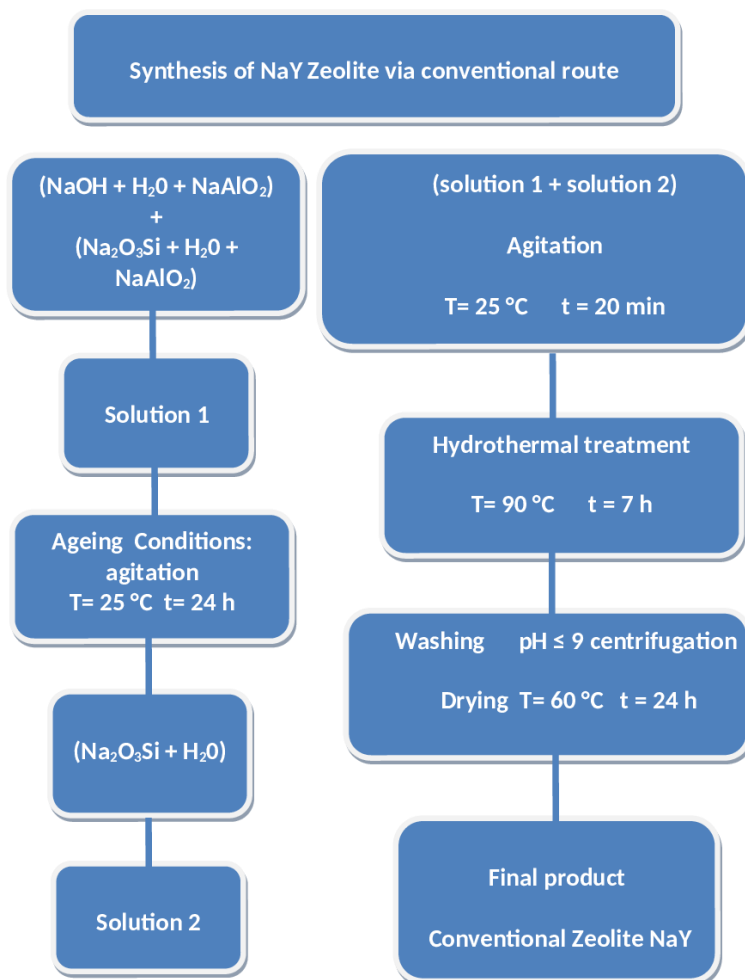


Figure 3 Stages of synthesis of zeolite NaY conventional route.

2.5 Synthesis of NaY Zeolite Via Sustainable Route (NaY_V)

Following all conventional synthesis procedures and replacing sodium silicate with sustainable silica (vermiculite clay after acid treatment and primary treatment).

The steps to be followed in synthesizing sustainable NaY zeolite are shown in the diagram in Figure 4.

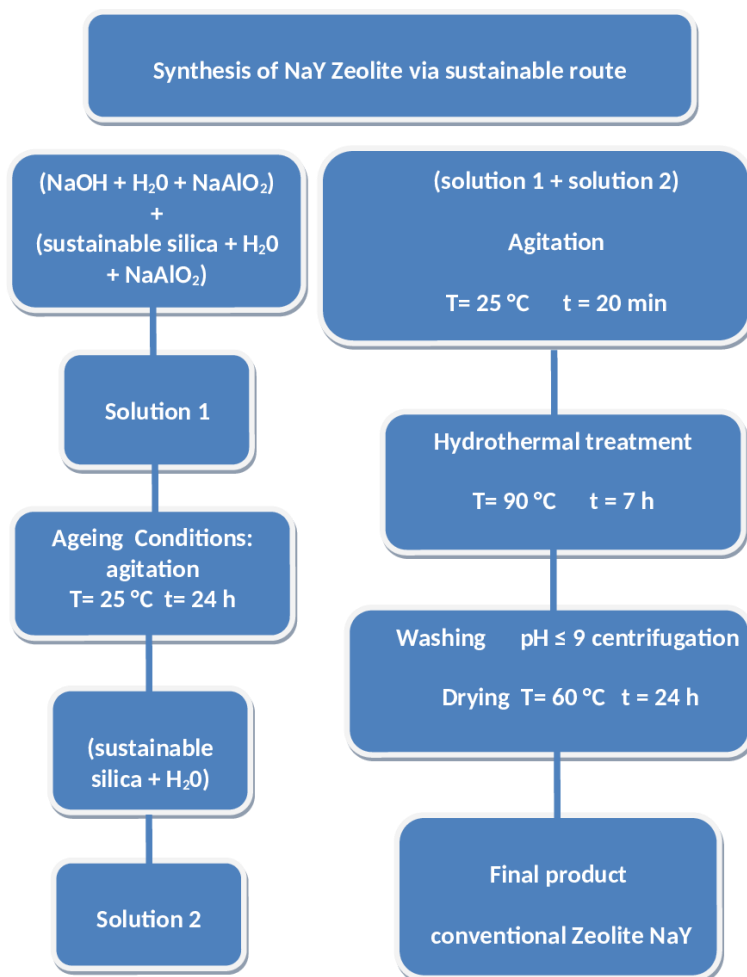


Figure 4 Stages of synthesis of zeolite NaY sustainable route.

The sample was named NaY_V zeolite, taking into account the sustainable method used.

2.6 Post Synthesis Modification of NaY Zeolite with CTABr Surfactant

According to the authors, the value of the cation exchange capacity of zeolite Y is 2.5 meq/g [26].

NaY zeolite conventional modified with CTABr was obtained by subjecting NaY_C zeolite to the ion exchange reaction [27]. A solution of 0.1 mol/L [CTABr] was used. To perform the exchange, this solution was added with stirring to 2 g of NaY_C zeolite at room temperature to a volume de solution [0.1 mol/L CTABr] of 100 mL. After 24 h, the solid was separated by filtration, washed with deionized water, and dried at 60°C for 24 h. The sample was named NaY_C_CTABr zeolite.

The steps to be followed in the ion exchange reaction are shown in the diagram in Figure 5.

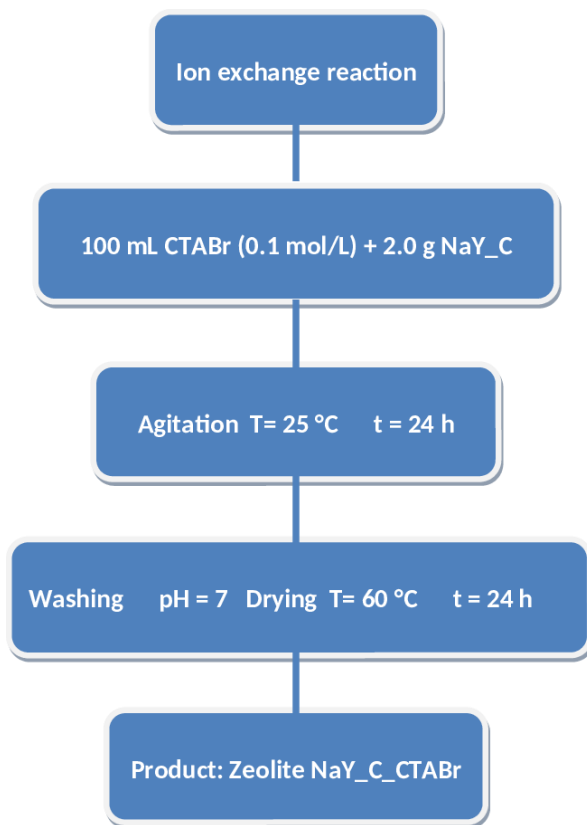


Figure 5 Diagram for ion exchange reaction (NaY_C).

2.7 Post Synthesis Modification of NaY_V Zeolite with CTABr Surfactant

The modification with CTABr was the same as that used in the previous section (2.6). The sample was named NaY_V_CTABr zeolite.

The steps to be followed in the ion exchange reaction are shown in the diagram in Figure 6.

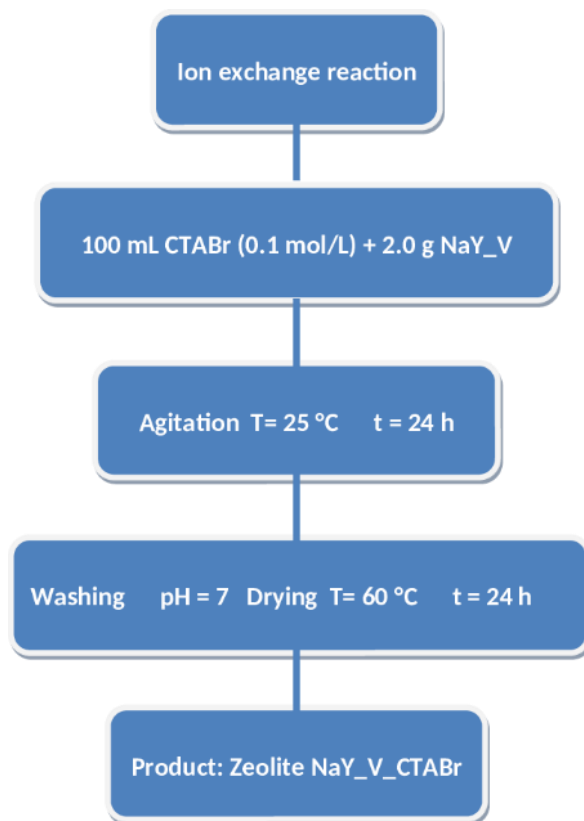


Figure 6 Diagram for ion exchange reaction (NaY_V).

2.8 Characterization

X-ray diffraction patterns were carried out on a Shimadzu XRD 6000 using Cu K α radiation at 40 kV/30 mA, with a goniometer velocity of 2°/min and step of 0.02° in the 2 θ range from 3.0° to 50.0°.

FTIR VERTEX 70 MODEL (Bruker) was used to obtain the infrared. The IR spectra were obtained at wavelengths in the 4000-400 cm⁻¹ range with a resolution of 4 cm⁻¹.

The elemental analysis was determined through energy-dispersive X-ray spectrophotometry in a Shimadzu EDX-700 instrument.

3. Results and Discussion

3.1 Vermiculite Clay

The vermiculite diffractogram is represented in Figure 7.

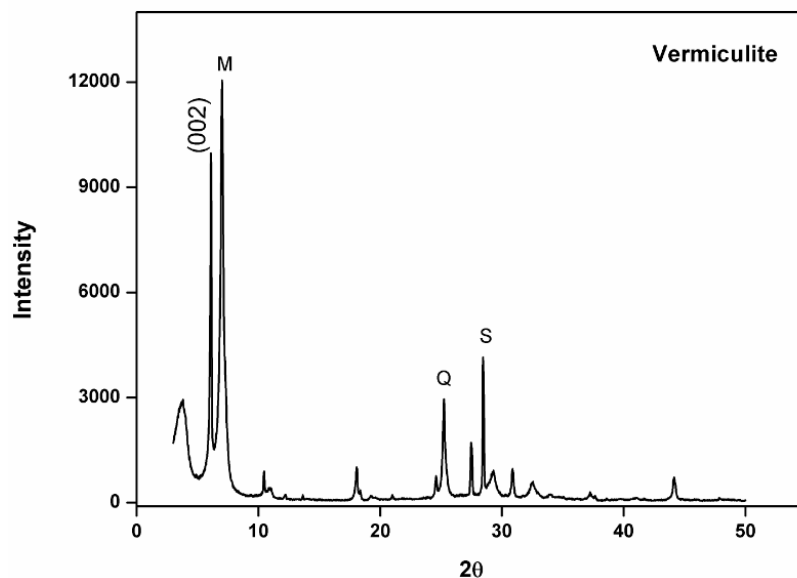


Figure 7 Diffratogram of vermiculite clay.

The X-ray diffractogram of vermiculite clay presents a characteristic peak of this clay mineral of the 2:1 type, presenting a crystalline structure with several reflections in the diffractogram, characteristic of vermiculite, presenting a broad reflection peak at $2\theta = 6.15^\circ$ attributed to the plane (002) with basal spacing $d_{002} = 14.39 \text{ \AA}$, indicating a two-water layer hydration state under Bragg's Law. In contrast, the reflection at approximately 7.02° refers to interlayer magnesium (M) cations that are dehydrated. The reflections close to 25.20° and 28.39° of lower intensities may be related to small amounts of quartz (Q) and sepiolite (S) impurities present in the vermiculite [28-30].

The results of chemical analyses for the vermiculite clay samples after acid and basic treatments are shown in Table 2.

Table 2 Chemical composition of the samples.

Compounds	Amount (%) In nature	Amount (%) After treatment
SiO ₂	42.80	45.30
Na ₂ O	1.00	47.30
MgO	28.20	-
Al ₂ O ₃	13.41	-
Fe ₂ O ₃	9.04	0.11
K ₂ O	3.38	0.77
P ₂ O ₅	0.08	2.50
MnO	0.12	-
TiO ₂	0.89	0.55
CaO	0.90	0.75
Impurities	-	2.06
Cl	-	0.65

The composition of vermiculite clay, in addition to silicon and aluminum oxides, has other common oxides, such as iron, potassium, manganese, titanium, and calcium. The significant

magnesium content (28.20%) of vermiculite confirms that this clay is of the magnesian type. The other sodium and phosphorus values found in this clay are close to those characterized by authors [31]. Vermiculites generally show a significant variation in chemical composition, even within the same deposit or occurrence. This variation is mainly due to differences in mineralization, alteration of biotite, mica, and degree of weathering [32].

According to the result after the chemical treatment of vermiculite explained in Table 2, an increase in the silicon content from 42.00% to 45.00% and a very significant increase in sodium oxide from 1.00% to 47.00% can be identified, coming from sodium hydroxide resulting from the primary treatment, as well as a reduction in the levels of other oxides that are not significant for the process of obtaining silica, such as potassium, iron, magnesium and other impurities, which could negatively interfere with the formation of zeolite generating competition with aluminum/silicon. Therefore, verifying that the acid and basic treatments were efficient is possible.

Figure 8 represents the image obtained by scanning electron microscopy (SEM) of the vermiculite clay at 2 KX magnification, showing the clay lamellae.

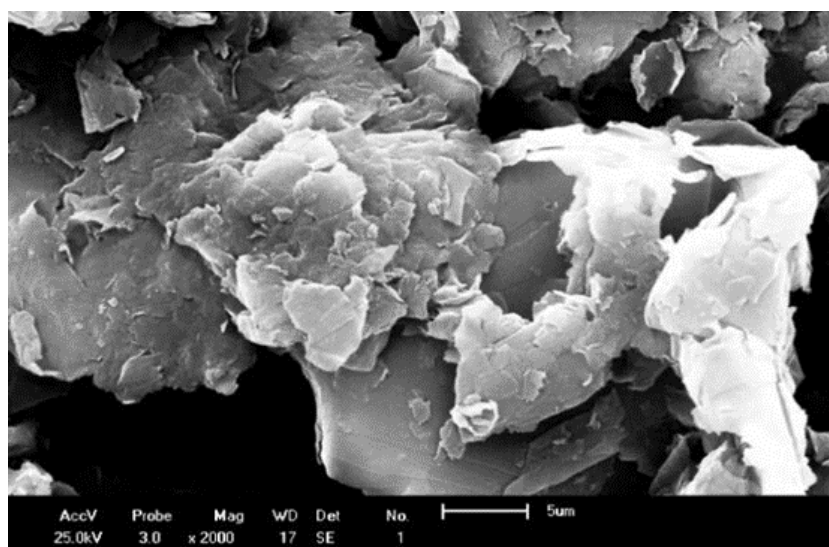


Figure 8 Image obtained by SEM of vermiculite clay.

One can see in Figure 8 the typical lamellar shape and the worm-shaped accordion structure, that is, a well-defined layered structure containing polygonal sheets with flaky edges and a significant layer of crystals. A morphology with compact structures arranged in irregularly shaped blocks with an average size of 7 μm [33], this morphology allows molecules of varying sizes to diffuse into the vermiculite and adsorb into its structure [34, 35].

Figure 9 shows FTIR spectra of vermiculite clay.

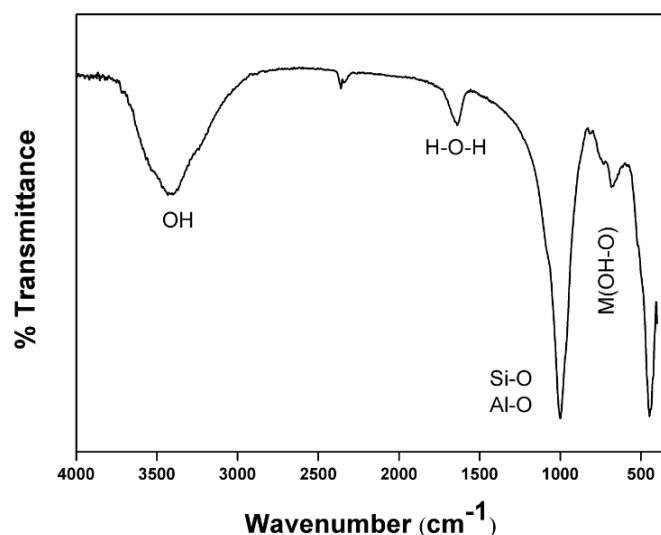


Figure 9 FTIR Spectra of the vermiculite clay.

The spectra in the infrared region of vermiculite clay illustrated in Figure 9 present broad and intense absorption bands at 3750-2900 cm⁻¹ attributed to stretching vibrations of the hydroxyl bond (O-H) and water adsorbed in the interlayer region [36]. The absorption band between 1630-1640 cm⁻¹ refers to the vibrational deformation of OH bonds in water [37]. The essential bands found for natural vermiculite within the 1300-500 cm⁻¹ range are related to the stretching of Si-O-Si and Si-O vibrations. The crew of most incredible intensity, which is found between 995 and 1070 cm⁻¹, represents the stretching of pulses of the Si-O and Al-O groups in the clay layers, and the weaker bands around 500-700 cm⁻¹ are attributed to the deformation vibrations of the M-OH or M-O bond, where M can be Al, Mg or Fe [38].

3.2 Synthesis of NaY Zeolite

Figure 10 and Figure 11 showed the XRD patterns of the prepared samples.

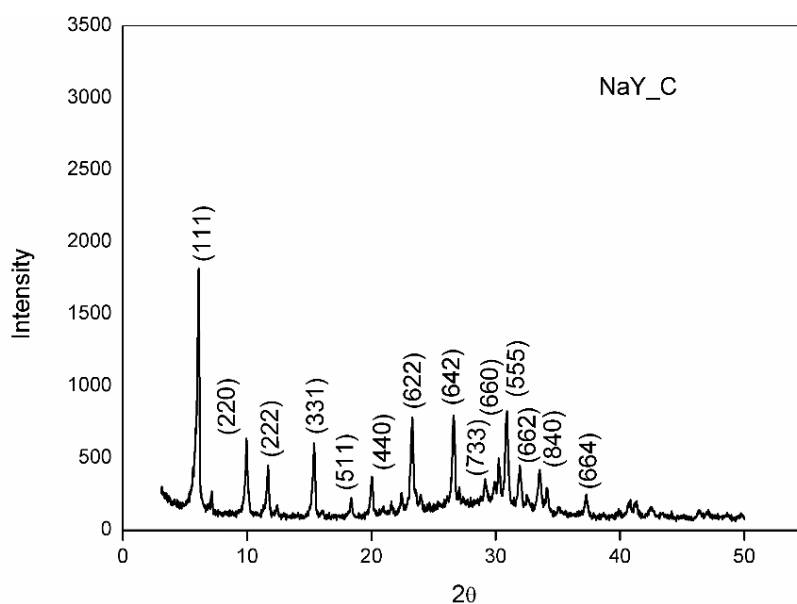


Figure 10 Diffratogram of NaY_C zeolite.

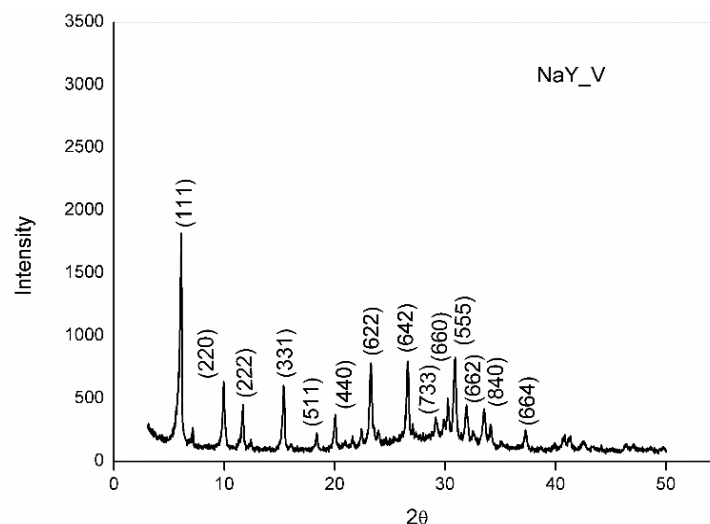


Figure 11 Diffratogram of NaY_V zeolite.

The NaY zeolite, derived from sodium silicate as illustrated in Figure 10, exhibited distinct peaks and defined boundaries. The zeolites acquired demonstrated high crystallinity and structural specifics within the 2θ range of 5 to 50° , aligning with the JCPDS 43-0168 standard form, consistent with existing literature [38].

Figure 11 depicts the X-ray diffractogram of NaY zeolite synthesized through a sustainable process utilizing vermiculite following acid and essential treatments. The predominant presence of the NaY phase is confirmed by characteristic peaks indicative of crystalline material, aligning with the JCPDS 43-0168 standard form. The X-ray diffraction analysis reveals that the sustainable route-synthesized NaY zeolite displays distinct peaks within the 2θ range of 5 to 50° , confirming the NaY zeolite formation. However, notable sodium content from the primary treatment and sodium aluminate is observed, accompanied by an amorphous region spanning 25 to 35° . Additionally, a reduction in peak intensity diminishes its crystallinity to 72% compared to the conventional method. The observed peak patterns align with existing literature on NaY zeolite synthesis [39, 40].

Table 3 displays the fluorescence results for the zeolite samples obtained through conventional and sustainable routes.

Table 3 Chemical composition of the zeolites NaY_C e NaY_V.

Compounds	Quantity (%) NaY_C	Quantity (%) NaY_V
SiO ₂	58.53	50.13
Al ₂ O ₃	34.85	33.51
Fe ₂ O ₃	-	0.09
Na ₂ O	6.40	15.81
MgO	-	0.37

As indicated in Table 3, the chemical composition of the NaY zeolite obtained through both silica source routes primarily comprised silica (SiO₂), alumina (Al₂O₃), and sodium oxide (Na₂O). In the case of NaY_V zeolite, the sodium oxide content exceeded that of NaY_C, which is attributable to the primary treatment applied to the silica source (vermiculite). Additionally, minor amounts of iron and magnesium oxides, each below 1.00%, were detected, originating from impurities in the raw

materials. These impurities tend to remain insoluble during the crystallization phase, potentially leading to the precipitation of undesired species. Such rainfall can potentially interfere with the zeolite formation process [41].

Figures 12 and 13 show the FTIR spectra of NaY_C zeolite and NaY_V zeolite.

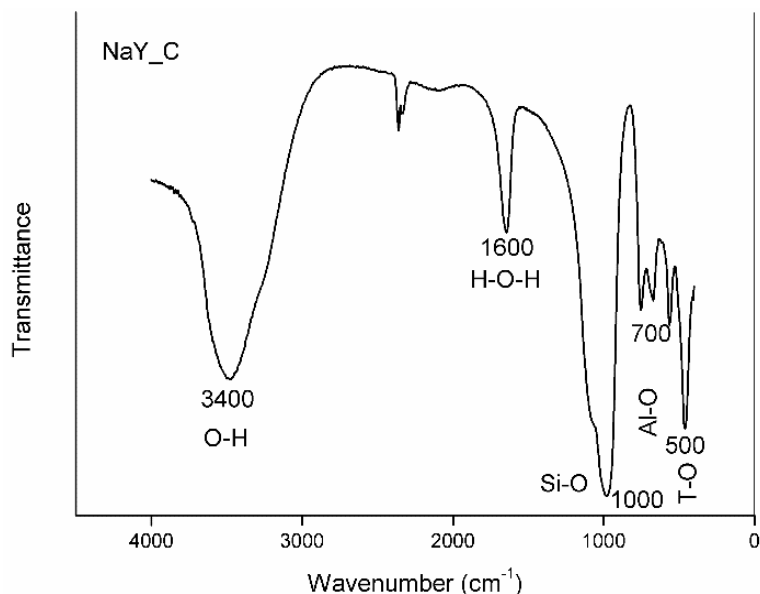


Figure 12 FTIR spectra of NaY_C zeolite.

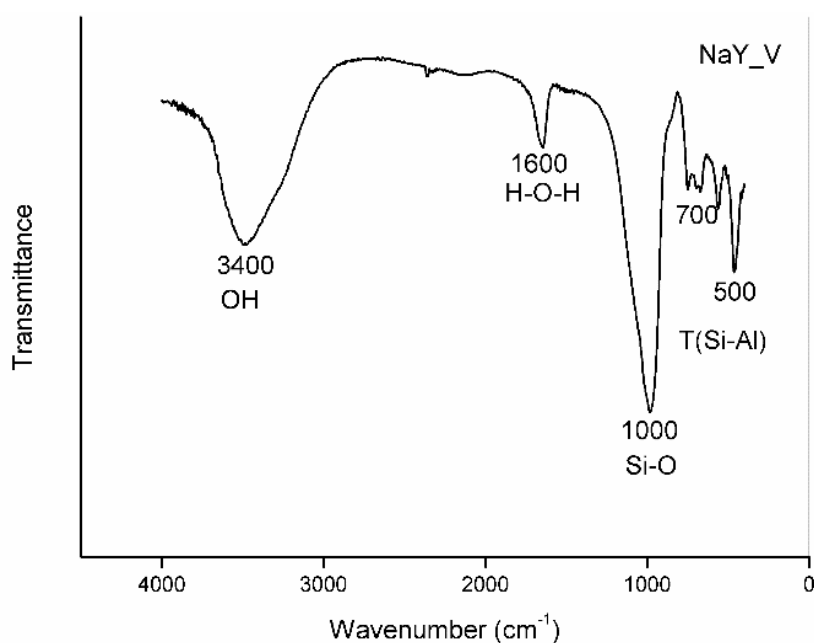


Figure 13 FTIR spectra of NaY_V.

The NaY zeolites obtained through both pathways exhibited characteristic bands corresponding to the aluminosilicate structure in the 1100-450 cm⁻¹ spectral region, associated with the Si-O and Al-O groups. The primary TO₄ units combine in various configurations to create distinct polyhedra and, consequently, diverse structures. Within the 1100-1000 cm⁻¹ range, the band is attributed to internal asymmetric stretching vibrations of the T(Si-Al)-O bonds, while the band spanning 500 to

700 cm^{-1} is linked to the symmetric stretching of the external tetrahedra in the NaY zeolite T-O [42-44]. The bar at 1600 cm^{-1} is associated with the angular deformation of the hydroxyl group and the bands in the 2400-2500 cm^{-1} range result from the symmetric and asymmetric stretching of C-H. Additionally, the crew at 3400 cm^{-1} corresponds to the OH hydroxyl groups originating from water molecules in the zeolite cavities [45].

Table 4 presents the data reported in the literature on the synthesis of aluminosilicate.

Table 4 Summary of the data reported on aluminosilicate synthesis.

Synthesis conditions/Method	Silica source	Formed phase	Ref.
110-150°C 6 h hydrothermal crystallization	Sodium metasilicate	NaY	[46]
Synthesis of potassium-Cesium aluminosilicate	Rice straw	RS-(K, Cs) AlSi_3O_8	[47]
90°C 7 h hydrothermal crystallization	Sodium metasilicate	NaY	This work
90°C 7 h hydrothermal crystallization	Vermiculite	NaY	This work

The results presented in Table 4 highlight the influence of the silica source on the formed phase in the preparation of aluminosilicate. It is apparent that various synthesis factors, including the aluminum source, crystallization time, and temperature, also play a significant role in determining the resulting phase. Consequently, alternative reagents such as silica derived from vermiculite demonstrate suitability for producing materials characterized by a cost-effective composition.

3.3 Post-Synthesis Modification (Ion Exchange Reaction)

The diffractograms of zeolites modified with the surfactant cetyltrimethylammonium bromide by cation exchange are represented in Figure 14 and Figure 15.

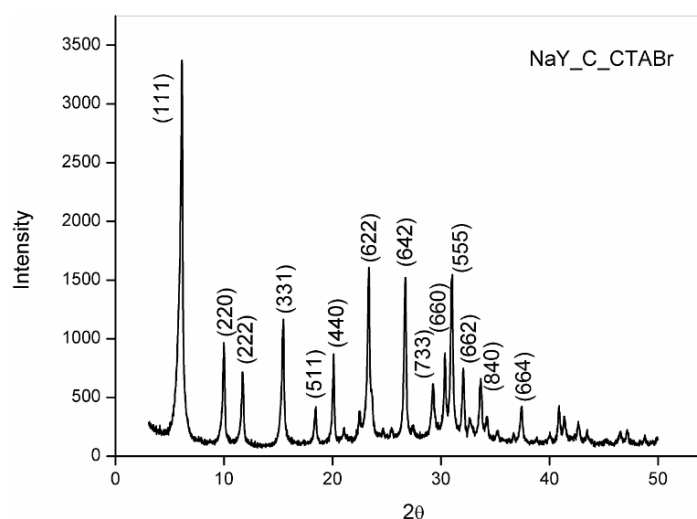


Figure 14 Diffratogram of zeolite NaY_C_CTABr.

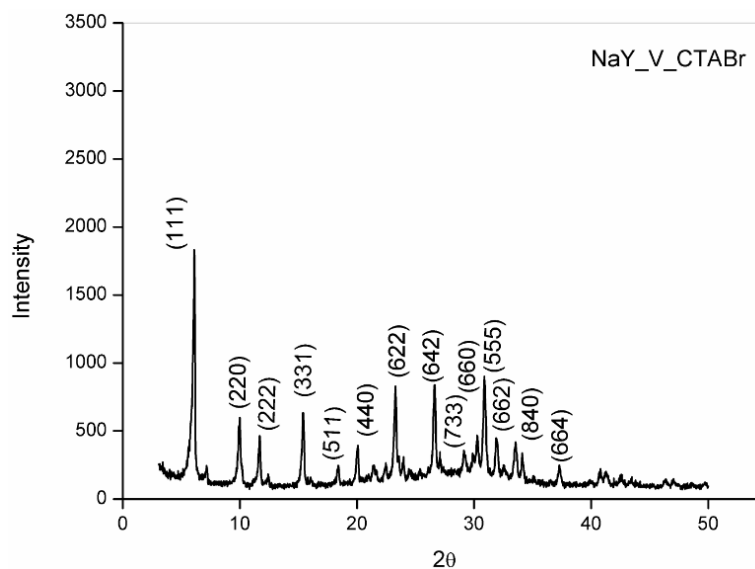


Figure 15 Diffraction pattern of zeolite NaY_V_CTABr.

As depicted in Figure 14 and Figure 15, the XRD patterns of the NaY zeolites exhibited no discernible changes following modification with the CTABr surfactant. In other words, the process of CTABr insertion did not impact the structure of the NaY zeolite, resulting in a consistent crystallinity of approximately 98% and 70%, respectively. This constancy in crystallinity is attributed to the unaltered Si/Al ratio [48]. The persistence of the intensity of the highest reflection peak in the (111) plane indicates that the surfactant was adsorbed within the internal region of the NaY zeolite [49].

Table 5 presents the outcomes of the chemical analyses conducted on zeolites subjected to modification with the surfactant cetyltrimethylammonium bromide (CTABr).

Table 5 Chemical composition of the zeolites modified with CTABr.

Compounds	Quantity (%) NaY_C_CTABr	Quantity (%) NaY_V_CTABr
SiO ₂	55.40	55.04
Br	0.76	0.68
Al ₂ O ₃	26.45	26.56
Fe ₂ O ₃	0.05	0.05
Na ₂ O	17.34	17.58

Table 5 reveals comparable values for aluminum oxides (Al₂O₃), sodium (Na₂O), iron (Fe₂O₃), and bromine (Br) in both adsorbent materials, along with closely aligned Si/Al molar ratios. The elevated sodium content is attributed to the NaY zeolites being synthesized in a sodium medium. The authors [46] propose that zeolite modification can induce desilication and dealumination processes involving the removal of silicon and aluminum atoms from the zeolite's structural network. However, the improvement with the CTABr surfactant did not exhibit these processes, as evidenced by the absence of changes in the chemical composition of zeolites, irrespective of the silica source used.

Figure 16 and Figure 17 depict the FTIR spectra of NaY zeolites following modification with the cetyltrimethylammonium bromide (CTABr) surfactant.

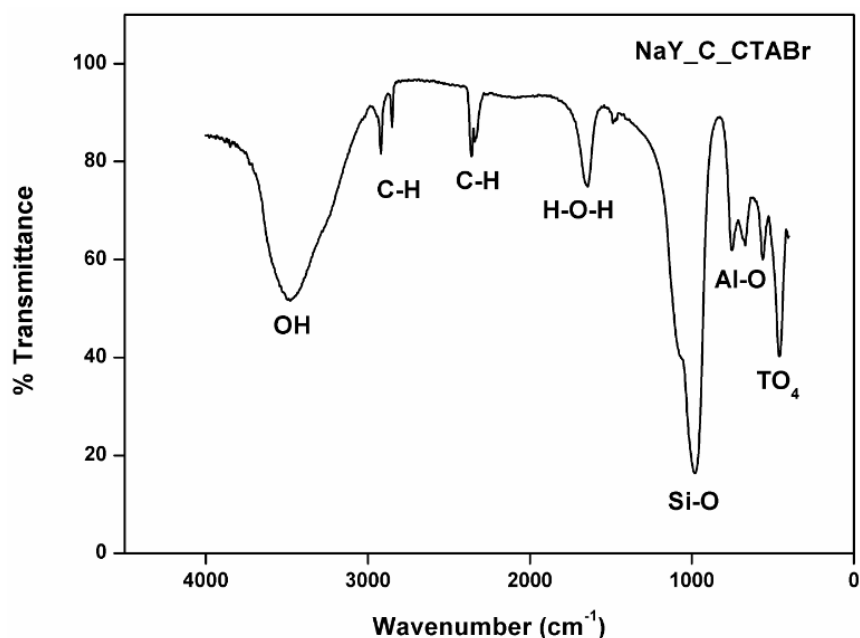


Figure 16 FTIR Spectra of the zeolite NaY_C_CTABr.

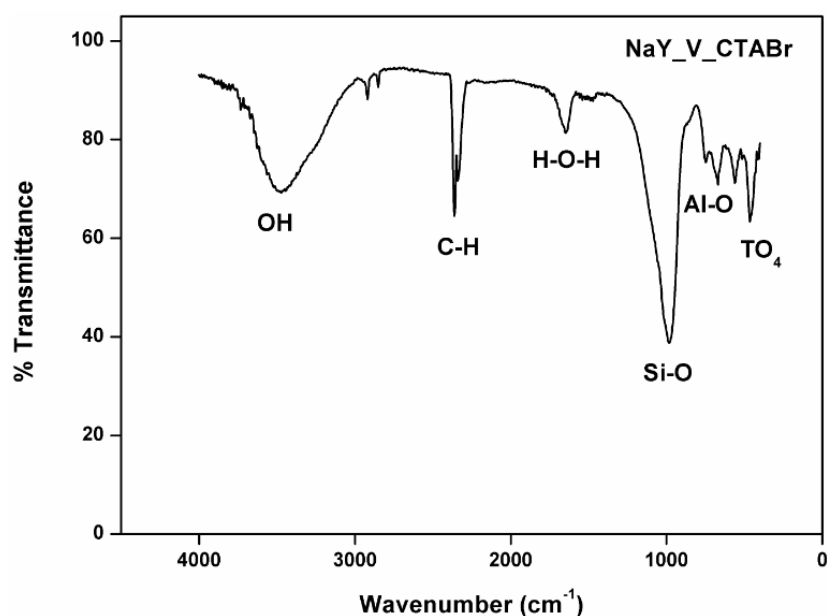


Figure 17 FTIR Spectra of the zeolite NaY_V_CTABr.

The FTIR spectra for CTAB-modified Zeolite NaY that have been compared with that of Zeolite NaY (Figure 12 and Figure 13) can be seen in Figure 16 and Figure 17.

The FTIR spectra at a region of 3000 to 2400 cm^{-1} for CTAB-modified Zeolite NaY (conventional and sustainable) bands emerged from the symmetric and asymmetric stretching of C-H attributed to the surfactant, signifying the effectiveness of the modification process in the NaY zeolite [49]. This suggests the existence of CTABr molecules on the surface of zeolite. CTABr consists of a positively charged ammonium hydrophilic head and a long hydrocarbon tail. The positively charged head can bind to the harmful sites of zeolite frameworks, adorning the outer layer with long chains of hydrocarbon tails. Consequently, the two extra peaks identified in the FTIR spectra were attributed to the C-H bonding within the extended hydrocarbon tails.

The primary characteristic bands of the zeolite, associated with Si-O and Al-O vibrations, were retained in the 480 to 1000 cm^{-1} range. Additionally, the band corresponding to the hydroxyl group persisted in the 3400 cm^{-1} region, indicating the structural stability of zeolites post-modification [50].

4. Conclusions

A distinctive crystalline structure typical of magnesite was confirmed after the characterization of vermiculite clay. The clay exhibited a lamellar shape with clearly defined layers, and the characteristic bands of vermiculite were identified. The primary mass loss observed in this clay mineral was attributed to water removal.

Utilizing diverse characterization techniques, the attainment of NaY zeolite was confirmed via both the conventional and sustainable routes, with preserved structural properties. Employing the sustainable way for NaY zeolite synthesis proved to yield a material with a low production cost while maintaining properties comparable to those synthesized conventional.

The structural integrity of NaY zeolites remained intact following the modification process involving the surfactant Cetyltrimethylammonium Bromide (CTABr). This underscores the zeolites' structural stability and affirms the efficacy of the modification process.

Acknowledgments

The authors gratefully acknowledge to the Coordenação de Aperfeiçoamento de Pessoal de Nível Superior (CAPES) for the financial support. We thank Laboratory of Multifunctional Materials and Nanocomposites LAMMEN-ECT UFRN for the FTIR analysis.

Author Contributions

Thiago R. B. Barros: Investigation, Formal analysis, Writing - Original Draft; Thianne S. B. Barbosa: Investigation, Formal analysis; Meiry G. F. Rodrigues: Conceptualization, Formal analysis, Funding acquisition, Writing - Review & Editing.

Funding

Coordenação de Aperfeiçoamento de Pessoal de Nível Superior (CAPES).

Competing Interests

The authors have declared that no competing interests exist.

Additional Materials

The following additional materials are uploaded at the page of this paper.

1. Table S1: Crystallographic parameters of NaY zeolites.
2. Table S2: Crystallographic parameters of NaY zeolites.

References

1. Marsh GP. *Man and nature: Or, physical geography as modified by human action*. Cambridge, MA, US: Belknap Press of Harvard University Press; 1864. pp. 149-156.
2. National Research Council of the National Academies. *Sustainability and the U.S. EPA*. Washington, DC, US: The National Academies Press; 2011. doi: 10.17226/13152.
3. Li Y, Li L, Yu J. Applications of zeolites in sustainable chemistry. *Chem*. 2017; 3: 928-949.
4. El Kordy A, Elgamouz A, Lemdek EM, Tijani N, Alharthi SS, Kawde AN, et al. Preparation of sodalite and faujasite clay composite membranes and their utilization in the decontamination of dye effluents. *Membranes*. 2021; 12: 12.
5. Lahnafi A, Elgamouz A, Tijani N, Jaber L, Kawde AN. Hydrothermal synthesis and electrochemical characterization of novel zeolite membranes supported on flat porous clay-based microfiltration system and its application of heavy metals removal of synthetic wastewaters. *Microporous Mesoporous Mater*. 2022; 334: 111778.
6. Breck DW. *Zeolite molecular sieves: Structure, chemistry, and use*. Hoboken, NJ, US: John Wiley & Sons; 1974.
7. Rožić M, Šipušić ĐI, Sekovanić L, Miljanić S, Čurković L, Hrenović J. Sorption phenomena of modification of clinoptilolite tuffs by surfactant cations. *J Colloid Interface Sci*. 2009; 331: 295-301.
8. Nezamzadeh Ejhieh A, Badri A. Application of surfactant modified zeolite membrane electrode towards potentiometric determination of perchlorate. *J Electroanal Chem*. 2011; 660: 71-79.
9. Salim MM, Ahmad N, Malek NN. Review of modified zeolites by surfactant and silver as antibacterial agents. *J Adv Res Mater Sci*. 2017; 36: 1-20.
10. Bergaya F, Lagaly G. *Handbook of clay science*. 2nd ed. Oxford, UK: Elsevier Science; 2013.
11. Souza Santos P. *Ciência e tecnologia de argilas*. 2nd ed. São Paulo, SP, US: Edgard Blücher; 1989.
12. Grim RE. *Clay mineralogy*. 2nd ed. New York, US: McGraw Hill; 1968.
13. Joseph IV, Tosheva L, Miller G, Doyle AM. FAU-type zeolite synthesis from clays and its use for the simultaneous adsorption of five divalent metals from aqueous solutions. *Materials*. 2021; 14: 3738.
14. Zang J, Yu H, Liu G, Hong M, Liu J, Chen T. Research progress on modifications of zeolite Y for improved catalytic properties. *Inorganics*. 2023; 11: 22.
15. de Paula GM, Lima LA, Freire Rodrigues MG. SBA-15 molecular sieve using clay as silicon sources. In: *Materials Science Forum*. Stafa-Zurich, Switzerland: Trans Tech Publications; 2014. pp. 116-120.
16. Lima LA, Menezes VM, Freire Rodrigues MG. Use residue of bagasse sugar cane in synthesis of molecular sieve MCM-41. In: *Materials Science Forum*. Stafa-Zurich, Switzerland: Trans Tech Publications; 2014. pp. 95-99.
17. da Silva VJ, Freire Rodrigues MG. Synthesis and characterization of ZSM-5 zeolite using kaolin as Si and Al source. In: *Materials Science Forum*. Stafa-Zurich, Switzerland: Trans Tech Publications; 2015. pp. 651-656.
18. dos Santos ER, Sousa AB, Leite RC, Laborde HM, Menezes RR, Freire Rodrigues MG. Preparation of zeolite MCM-22 using the rice husk ash as silica source. In: *Materials Science Forum*. Stafa-Zurich, Switzerland: Trans Tech Publications; 2015. pp. 646-650.

19. Silva VJ, Rodrigues JJ, Soares RR, Napolitano MN, Rodrigues MG. Cobalt supported on ZSM-5 zeolite using kaolin as silicon and aluminum sources for Fischer-Tropsch synthesis. *Braz J Pet Gas*. 2013; 7: 83-94.
20. Medeiros de Paula G, do Nascimento Rocha de Paula L, Freire Rodrigues MG. Production of MCM-41 and SBA-15 hybrid silicas from industrial waste. *Silicon*. 2022; 14: 439-447.
21. de Paula LN, de Paula GM, Rodrigues MGF. Adsorption of reactive blue BF-5G dye on MCM-41 synthesized from Chocolate clay. *Cerâmica*. 2020; 66: 269-276.
22. De Paula GM. Preparação dos catalisadores MoO₃/MCM-41 e MoO₃/SBA-15 com fontes alternativas de sílica destinados à reação de transesterificação do óleo de soja. República Federativa do Brasil: Universidade Federal de Campina Grande; 2017.
23. Lima WS, de Brito AL, Freire Rodrigues MG, Mota MF, Silva MM. Characterization of national clays after acid treatment and thermal. In: *Materials Science Forum*. Stafa-Zurich, Switzerland: Trans Tech Publications; 2015. pp. 662-666.
24. De Paula GM, Rodrigues MGF. Processo de produção da peneira molecular SBA-15 a partir de argila chocolate, cinzas de cascas de arroz e cinzas de bagaço de cana-de-açúcar. BR 102017022940-8; 2019.
25. Ginter DM, Bell AT, Radke CJ. *Synthesis of Microporous Materials: Molecular sieves*. New York, NY, US: Van Nostrand Reinhold; 1992.
26. Hashemi MS, Eslami F, Karimzadeh R. Organic contaminants removal from industrial wastewater by CTAB treated synthetic zeolite Y. *J Environ Manage*. 2019; 233: 785-792.
27. Malek NA, Malek NS. Modification of synthetic zeolites by quaternary ammonium compounds and its antibacterial activity against *Bacillus subtilis*. *APCBEE Procedia*. 2012; 3: 134-139.
28. Wang CF, Gu HZ, Zhou F. Investigation of inorganic-intercalated vermiculite by X-ray diffraction. *Adv Mater Res*. 2011; 177: 602-605.
29. Valášková M, Martynková GS, Raaen AM. *Clay minerals in nature: Their characterization, modification and application*. London, UK: IntechOpen; 2012.
30. Dixon JB, Schulze DG. *Soil mineralogy with environmental applications*. Soil mineralogy with environmental applications. Madison, WI, US: Soil Science Society of America Inc.; 2002.
31. Marcos C, Arango YC, Rodriguez I. X-ray diffraction studies of the thermal behaviour of commercial vermiculites. *Appl Clay Sci*. 2009; 42: 368-378.
32. de Queiroga LN, Soares PK, Fonseca MG, de Oliveira FJ. Experimental design investigation for vermiculite modification: Intercalation reaction and application for dye removal. *Appl Clay Sci*. 2016; 126: 113-121.
33. Yu XB, Wei CH, Ke L, Wu HZ, Chai XS, Hu Y. Preparation of trimethylchlorosilane-modified acid vermiculites for removing diethyl phthalate from water. *J Colloid Interface Sci*. 2012; 369: 344-351.
34. El Mouzdahir Y, Elmchaouri A, Mahboub R, Gil A, Korili SA. Synthesis of nano-layered vermiculite of low density by thermal treatment. *Powder Technol*. 2009; 189: 2-5.
35. Silva FM, Barros TR, Barbosa TS, Lima EG, Barbosa TL, Rodrigues MG. Expansibility of vermiculite (Santa Luzia, Brazil) irradiated with microwave. *Cerâmica*. 2021; 67: 230-235.
36. Farmer VT, Russell JD. The infra-red spectra of layer silicates. *Spectrochim Acta*. 1964; 20: 1149-1173.
37. Ritz M, Zdrálková J, Valášková M. Vibrational spectroscopy of acid treated vermiculites. *Vib Spectrosc*. 2014; 70: 63-69.

38. Medri V, Papa E, Mazzocchi M, Laghi L, Morganti M, Francisconi J, et al. Production and characterization of lightweight vermiculite/geopolymer-based panels. *Mater Des.* 2015; 85: 266-274.
39. Dabbawala AA, Tzitzios V, Sunny K, Polychronopoulou K, Basina G, Ismail I, et al. Synthesis of nanoporous zeolite-Y and zeolite-Y/GO nanocomposite using polyelectrolyte functionalized graphene oxide. *Surf Coat Technol.* 2018; 350: 369-375.
40. Azat S, Korobeinyk AV, Moustakas K, Inglezakis VJ. Sustainable production of pure silica from rice husk waste in Kazakhstan. *J Clean Prod.* 2019; 217: 352-359.
41. Bortolatto LB, Santa RA, Moreira JC, Machado DB, Martins MA, Fiori MA, et al. Synthesis and characterization of Y zeolites from alternative silicon and aluminium sources. *Microporous Mesoporous Mater.* 2017; 248: 214-221.
42. Taufiqurrahmi N, Mohamed AR, Bhatia S. Nanocrystalline zeolite Y: Synthesis and characterization. *IOP Conf Ser Mater Sci Eng.* 2011; 17: 012030.
43. Oliveira TG, Machado SW, Santos SC, Souza MJ, Pedrosa AM. Adsorção de CO₂ em peneiras moleculares micro e mesoporosas. *Química Nova.* 2014; 37: 610-617.
44. Huo Z, Xu X, Lv Z, Song J, He M, Li Z, et al. Thermal study of NaP zeolite with different morphologies. *J Therm Anal Calorim.* 2013; 111: 365-369.
45. Kulprathipanja S. *Zeolites in Industrial Separation and Catalysis.* Weinheim, Germany: Wiley-VCH Verlag GmbH & Co. KGaA; 2010.
46. Shichalin OO, Papynov EK, Nepomnyushchaya VA, Ivanets AI, Belov AA, Dran'kov AN, et al. Hydrothermal synthesis and spark plasma sintering of NaY zeolite as solid-state matrices for cesium-137 immobilization. *J Eur Ceram Soc.* 2022; 42: 3004-3014.
47. Panasenko AE, Shichalin OO, Yarusova SB, Ivanets AI, Belov AA, Dran'kov AN, et al. A novel approach for rice straw agricultural waste utilization: Synthesis of solid aluminosilicate matrices for cesium immobilization. *Nucl Eng Technol.* 2022; 54: 3250-3259.
48. Mirzaei N, Hadi M, Gholami M, Fard RF, Aminabad MS. Sorption of acid dye by surfactant modified natural zeolites. *J Taiwan Inst Chem Eng.* 2016; 59: 186-194.
49. Pukcothanung Y, Siritanon T, Rangsriwatananon K. The efficiency of zeolite Y and surfactant-modified zeolite Y for removal of 2,4-dichlorophenoxyacetic acid and 1, 1'-dimethyl-4, 4'-bipyridinium ion. *Microporous Mesoporous Mater.* 2018; 258: 131-140.
50. Lin J, Zhan Y. Adsorption of humic acid from aqueous solution onto unmodified and surfactant-modified chitosan/zeolite composites. *Chem Eng J.* 2012; 200: 202-213.